Theor Appl Climatol (2016) 124:497–515
DOI 10.1007/s00704-015-1416-z

ORIGINAL PAPER

Modeling and imaging land-cover influences on air temperature in and near Baltimore, MD

Gordon M. Heisler · Alexis Ellis · David J. Nowak · Ian Yesilonis

Received: 4 December 2012 / Accepted: 20 February 2015 / Published online: 25 March 2015

Abstract Over the course of 1681 hours between May 5 and September 30, 2006, air temperatures measured at the 1.5-m height at seven sites in and near the city of Baltimore, MD were used to empirically model $\Delta \widehat{T}_{R\text{-}p}$, the difference in air temperature between a site in downtown Baltimore and the six other sites. Variables in the prediction equation included difference between the downtown reference and each of the other sites in upwind tree cover and impervious cover as obtained from 10-m resolution geographic information system (GIS) data. Other predictor variables included an index of atmospheric stability, topographic indices, wind speed, vapor pressure deficit, and antecedent precipitation. The model was used to map predicted hourly $\Delta \widehat{T}_{R\text{-}p}$ across the Baltimore region based on hourly weather data from the airport. Despite the numerous sources of variability in the regression modeling, the method produced reasonable map patterns of $\Delta \widehat{T}_{R\text{-}p}$ that, except for some areas evidently affected by sea breeze from the Chesapeake, closely matched results of mesoscale modeling. Potential applications include predictions of the effect of changing tree cover on air temperature in the area.

1 Introduction

Despite being the subject of vast numbers of investigations over the last several decades, methods for evaluating urban temperature patterns continue to be of scientific interest because of the possibility of using urban planning to ameliorate excessive temperatures (Grimmond et al. 2010). Studies have been published for hundreds of cities worldwide, including almost every major city in Europe, North America, and East Asia (Grimmond 2011; Heisler and Brazel 2010; Roth 2007; Roth et al. 2011; Stewart 2011).

This plethora of studies has left gaps in knowledge about the effects on air temperature of certain differences in urban structure, including how to quantify the effects of differences in vegetation, especially differences in tree cover. Although high building and road density generally lowers the opportunity for high tree cover, in many developed areas, particularly in areas of single-family homes, a wide range of tree cover is possible. Few studies have sampled the full range of vegetation differences that are possible within a given built structure.

There are multiple concerns about urban temperature that create a need for tools to predict urban temperature patterns in time and space. Over much of the world, high temperatures in cities are a health risk for the ever-increasing human populations. Other concerns about urban climate include energy use for space conditioning of buildings, high peak-power demands for air conditioning, the relationship of urban climate to global climate change (Mills 2007; Oke 1997; Roth et al. 2011), and high temperatures increasing ozone production

Electronic supplementary material The online version of this article (doi:10.1007/s00704-015-1416-z) contains supplementary material, which is available to authorized users.

G. M. Heisler (✉) · D. J. Nowak
Northern Research Station, USDA Forest Service, c/o State University of New York, College of Environmental Science and Forestry, 5 Moon Library, 1 Forestry Drive, Syracuse, NY 13210, USA
e-mail: gmheisler@fs.fed.us

A. Ellis
The Davey Institute, c/o USDA Forest Service, 5 Moon Library, 1 Forestry Drive, Syracuse, NY 13210, USA

I. Yesilonis
Northern Research Station, USDA Forest Service, c/o Baltimore Ecosystem Study, 5523 Research Park, Suite 350, Baltimore, MD 21228, USA

(Nowak et al. 2000; Taha 1996). Both direct and indirect effects of temperature changes influence human health and comfort. Several studies have demonstrated that temperature threshold exceedance and air pollution in cities exacerbate human discomfort, heat-related health incidences, and mortality (Baker et al. 2002; Grass and Crane 2008; Harlan et al. 2006; Kalkstein and Smoyer 1993).

For tourist information and promotion, city climate is generally reported by data from the main weather station, usually an airport, which may have significantly more or less disagreeable climate than most of the city (Hartz et al. 2006). Given knowledge of temperatures in different parts of a city, the temperature influence on human comfort can be quantitatively modeled (Hartz et al. 2006; Heisler and Wang 2002; Matzarakis et al. 2007), so that more accurate indices of comfort in a city are possible.

Any successful method of modeling urban temperatures will account, either directly or indirectly, for the physical processes that create differences in temperature across the city and its surrounding area. These processes are hypothesized (Brazel and Quatrocchi 2005; Oke 1979) to include: (1) anthropogenic heat from buildings (Sailor 2011), (2) greater than normal shortwave radiation absorption due to canyon geometry (Oke 2011), (3) differences in net longwave loss due to differences in sky view factor by canyon geometry (Oke 1987), (4) greater urban daytime heat storage and nocturnal release due to differences in thermal admittance of building materials compared to rural land cover (Cleugh and Grimmond 2012), (5) greater sensible heat flux in more urbanized areas due to decreased evaporation resulting from removal of vegetation and ground surface waterproofing by concrete and asphalt (Grimmond and Oke 1999), and (6) convergence of sensible heat due to reduction of wind speed in an urban canopy layer compared to an agricultural rural area (Comrie 2000). The successful model must also include the fact that all of these effects are minimized as cloud cover increases and synoptically forced wind speed increases (Morris et al. 2001).

Modeling of urban temperature regimes includes empirical regression methods, which permit an examination of the influences of tree and impervious cover at a relatively fine scale (Ellis 2009; Heisler et al. 2007, 2010), as compared to modeling of urban temperatures by mesoscale modeling (Georgescu et al. 2011; Rosenzweig et al. 2006; Taha 1996; Taha et al. 1997; Zhang et al. 2011). Regression models also offer the possibility of making predictions over a larger spatial domain and for a larger range of times than has sometimes been done by computational fluid dynamics models (Ashie and Konob 2011) or numerical modeling (Krayenhoff and Voogt 2010; Krayenhoff et al. 2009), though domains of numerical model studies are increasing. The empirical methods also permit consideration of the lower urban canopy layer atmospheric urban heat island, in contrast to the upper urban surface "skin" temperature that is measured by remote sensing of thermal emissions from satellites or aircraft (Voogt and Oke 2003), which also is available for only limited times. On the other hand, empirical methods have the challenge of dealing with collinearity in the dependent variables and the concern that model results should not be extrapolated beyond the range of measurements of the independent variables. In the case of this study, that range of measurements includes the impervious cover, tree canopy cover, the topographic descriptors, and the ambient meteorological conditions—vapor pressure deficit and antecedent precipitation. Although atmospheric stability classes were not equally represented, at least the full range of classes was included.

The empirical model results permit several important applications. One is in picturing with relative ease and in relatively high resolution, the urban influences on predicted temperature in space and time using a GIS. Another is the possibility of estimating the effect of temporal changes in urban structure, for example changes in urban tree canopy cover. Another application is in defining the maximum urban heat island intensity, a fundamental goal of many urban climate studies (Oke 1973). Generally, the maximum urban heat island intensity ($maxT_{u\text{-}r}$) is estimated as the difference between the warmest point in a city and the temperature in a rural location. A common difficulty is that although temperature is available from somewhere within the city and also in a rural location, these points are not the very warmest and coolest locations. Our GIS maps permit predicting the warmest urban temperature to compare with either the coolest temperature in the modeling domain or the temperature in a particular land use, such as agricultural or forest.

The analysis in this paper is based on air temperature measurements at the 1.5-m height at seven stations in and near Baltimore, Maryland during the summer of 2006. Atmospheric stability, cloud cover, and wind speed were accounted for by airport weather data. Land cover was derived by GIS averaging of differences between the reference and other stations in upwind tree canopy, impervious cover, and water cover from light detection and ranging (LiDAR) data. Results are presented as maps of predicted temperature difference from the predicted warmest point within the modeling domain, which was invariably near the city center.

Our anticipated primary application of the analysis method is for evaluating urban forest effects on air temperature (Ellis 2009). Modifications to the urban forest by tree management have the potential for increasing air quality (Nowak et al. 2006), reducing energy use for building space conditioning (Heisler 1986; Simpson 2002), affecting human health and comfort (Hartz et al. 2006), and modifying sequestration of carbon (Nowak and Heisler 2010). Long-term trends in the urban heat island (UHI) in Baltimore have been described by Brazel et al (2000).

2 Methods

The study described here developed an equation for predicting air temperature differences, $\Delta \widehat{T}_{R\text{-}p}$ at the 1.5-m height above ground level (agl), where $\Delta \widehat{T}_{R\text{-}p}=T_R-T_{p,}$ T_p is temperature at any point in the modeling domain, and T_R is a measured reference temperature. The model method was empirical multiple linear regression analysis with the dependent variable, ΔT_m, being equivalent to $\Delta \widehat{T}_{R\text{-}p}$, except that ΔT_m was the measured difference between T_R, hourly temperature at the reference weather station, and T_s, temperature at other stations within the modeling domain. Predictor variables were derived from differences in land cover and topography along with forcing atmospheric conditions. Independent variables included: (1) difference between weather station sites in upwind land cover, (2) descriptors of topography around the sites, (3) a thermal stability index, (4) vapor pressure deficit, and (5) antecedent precipitation. The land-cover differences were from remotely sensed tree cover, impervious cover, and water cover over a range of distances upwind. Reference T_R was from a National Weather Service station in downtown Baltimore, and values of T_s were from six other weather stations within the modeling domain. Application of the model includes mapping $\Delta \widehat{T}_{R\text{-}p}$ across the Baltimore region. The current modeling analysis of $\Delta \widehat{T}_{R\text{-}p}$ was based on previous work for the Baltimore area (Ellis 2009; Heisler et al. 2007, 2010).

Our previous modeling studies for Baltimore also related temperature differences between points in urban areas to upwind land cover, modeled solar input, vapor pressure deficit, and antecedent precipitation. In the current study, additional predictor variables are considered along with methods to deal with the correlation between many of the potential independent variables. We also compare our model results to mesoscale model runs by Zhang et al. (2011).

2.1 Measurement sites

The size and shape of the modeling domain were chosen to include all of Baltimore, MD, along with the suburbs that are of most interest to the Baltimore Ecosystem Study (BES, http://www.beslter.org/), of which this study was a part. As a contribution to BES, a US National Science Foundation Long Term Ecological Research (LTER) site, we measured weather variables continuously at five locations near Baltimore. We also used data from two National Weather Service Automated Surface Observing System (ASOS) stations (Downtown and Airport, Table 1). The non-ASOS station locations were selected for purposes other than the particular analysis described here, so that although they represent a variety of land-use types, they are somewhat clustered with three stations being within about 1 km of each other and two others having only about 0.5 km between them (Fig. 1a). The clustering probably was not much of a problem regarding assumptions of regression analysis, but clustering and the type of sites selected did somewhat limit the range of the independent variables. For example, the site selection probably increased the range of elevations beyond what would have been the range if sites had been selected by a purely random method; two sites were near hill tops and three were in valleys near small streams.

The locations of the weather stations except at the airport Site 7 and the rural open Site 5 are decidedly not at sites like those recommended by Oke (2006) for urban climate studies, where microscale influences are minimized (see Oke (1987) for scale definition). Our interest in urban climate is to include the influences of finer scale urban structures—trees, buildings, grass, and impervious ground surfaces, so that station locations close to trees and buildings are acceptable. Unfortunately for the data used in this analysis, although Site 6 was close to a large building, it was not an inner-city street canyon. While city canyon sites were not sampled directly, Site 6 was within 1 km of the city center with tall buildings and street canyons. Except for the Woods site, which had a deciduous leaf litter layer, the weather station locations had short grass ground cover. However, except for the Woods Site, no site was more than 100 m from significant impervious cover.

Stewart and Oke (2012) describe and urge use of Local Climate Zones to categorize sites of measurements for urban canopy layer temperature analysis. They also suggest locating temperature measurement sites away from Zone borders. In our case, measurement sites were previously decided, especially for the ASOS stations, and one of these, the Downtown site, was near the edge of several LCZs. Estimates of LCZs are included in the last column of Table 1, with two classifications given for the Downtown site, 4 (Open highrise) and G (Water), because the station is within 60 m of the Baltimore Inner Harbor. Other sites were 5_B (Open midrise with scattered trees) for Site 1, 9_B (Sparsely built with scattered trees) for Site 2, 6_B (Open lowrise with scattered trees) for Site 3, A (Dense trees) for 4, and D (Low plants) for Sites 5 and 7.

Urban air temperatures within the canopy layer are strongly related to sky view through the influence of trees and buildings on solar irradiance and thermal radiation exchange with the sky (Lindberg and Grimmond 2011; Oke 1987). Sky view factor was not explicitly included in the ΔT modeling here, but we did evaluate sky view from 180° hemispherical photos taken looking directly upward from the 1-m height agl at each site except at the airport, Site 7, where sky view was assumed to be 98 %. Sky view values were derived from the hemispherical photos by analysis with the Gap Light Analyzer (GLA) program (http://www.ecostudies.org/gla/). Measured sky view percentages ranged from 6 % at the woods, Site 4, to 96 % at rural open, Site 5 (Table 1).

Table 1 Weather station sites, sky view, topographic indices, and Local Climate Zones. See text for full definitions of columns

Site	Sky view %	Station elevation, E_s m	$(E_s\text{-}E_{L2})$[a] m	E_{RL2}[b]	$(E_{H2}\text{-}E_s)$[c] m	E_{RH2}[d]	D_{A2}[e] m	D_{T2}[f] m	Steepest slope[g], deg.	LCZ[h]
1 Apartment	31	101	40	0.45	49	0.55	18	27	26	5_B
2 Resid. with overstory	25	145	108	0.96	4	0.04	104	0	68	9_B
3 Resid. open	37	103	65	0.58	47	0.42	38	19	18	6_B
4 Woods	6	139	16	0.22	58	0.78	4	45	33	A
5 Rural open	96	157	35	0.53	32	0.47	19	15	21	D
6 Downtown	78	3	3	0.11	34	0.89	0	30	24	4, G
7 Airport	98	42	26	0.57	19	0.43	15	8	26	D

[a] Height in meters above lowest elevation within 2 km of the site

[b] Ratio of height of the site above the lowest elevation within a 2-km radius of the site to total relief within 2 km, $(E_s - E_{L2})/(E_{H2} - E_{L2})$

[c] Height in meters below the highest elevation within 2 km

[d] Ratio of site elevation below the highest elevation within 2 km to total relief within 2 km, $(E_{H2} - E_s)/(E_{H2} - E_{L2})$

[e] Cold Drainage Away, Eq. 1 in text

[f] Cold Drainage Toward, Eq. 2 in text

[g] Slopes from USGS National Elevation Dataset (NED) with about 10-m resolution

[h] Local Climate Zone of Stewart and Oke (2012)

Figure 1b shows the larger regional setting of our study area. The map shows the domain of our modeling along with the partly overlapping domain of a mesoscale modeling study by Zhang et al. (2011) that we compare to our results. Possible regional influences on Baltimore area temperatures include sea breeze effects from Chesapeake Bay and long-distance advection from the Washington, DC area.

2.2 Measurements and instrumentation

The observations of ΔT_m covered the period from May 5, 2006 to September 30, 2006. Trees were essentially in full leaf during this time. For the analysis, we used only hours that had temperature measurements for all sites.

At the non-ASOS sites, instrument packages with data loggers recorded wind speed, wind direction, and air temperature, but the sensors differed somewhat. At all sites, including the ASOS sites, air temperature (T_m, which consists of T_R and T_s) is measured at 1.5 m above ground. At Sites 1, 3, and 4 (Fig. 1a), T_m is measured with thermistors in naturally ventilated Gill-type radiation shields (Table 2). With these systems, maximum errors with high radiation loads and low wind speeds probably exceed 1 °C (Gill 1983). Station 2 measured T_m with a thermistor in a double-tube, power-aspirated radiation shield for which maximum combined electronic and radiation errors probably are ±0.3 °C. The Rural Open Site 5 is the primary weather station for the BES LTER site (Heisler et al. 2000). Here, a platinum resistance thermometer (RTD) device in a double-tube, fan-aspirated radiation shield (REBS Radiation Energy Balance, Inc., Bellvue, WA) measures air temperature with maximum errors of about ±0.1 °C. The ASOS sites have temperature sensors in well-protected and aspirated radiation shields, but reporting resolution is only to the nearest 1 °F (0.55 °C).

The non-ASOS sites sample air temperature at 5-s intervals and average over 15 min. For this analysis, the averages from 15 min before the hour to the top of each hour were compared to data from the ASOS sites, which measure at 10-s intervals and record average temperature and relative humidity over a 2-min period at 6 to 8 min before each hour.

The precipitation measurement was also derived from the Airport ASOS station, where measurements are made with a tipping-bucket gage with a 12-in (305-mm) orifice. In addition to current precipitation during the previous hour, antecedent precipitation variables consisted of total precipitation during the last 24 h, the last 7 days, and the last 28 days.

2.3 Atmospheric stability

The ΔT variables ($\Delta \widehat{T}_{R\text{-}p}$ or ΔT_m) are essentially a manifestation of the UHI effect. It is well-known that the UHI is greatest with light winds and clear skies at night (Oke 1982). The effect is reduced by high wind speed and cloud cover. Wind speed and cloud cover also affect atmospheric thermal stability (Stull 2000). Our method of modeling ΔT makes use of the fact that wind speed and cloud cover are incorporated in indices of atmospheric stability.

In the regression analysis to predict ΔT, we combined the forcing effect of cloud cover and wind speed by the Turner stability index, S (Panofsky and Dutton 1984; Turner 1961, 1964), that is derived from standard airport weather observations of wind speed at 10 m agl and cloud cover including cloud height (National Climatic Data Center 2011). Turner Class is based on wind speed and a "Net Radiation Index" calculated

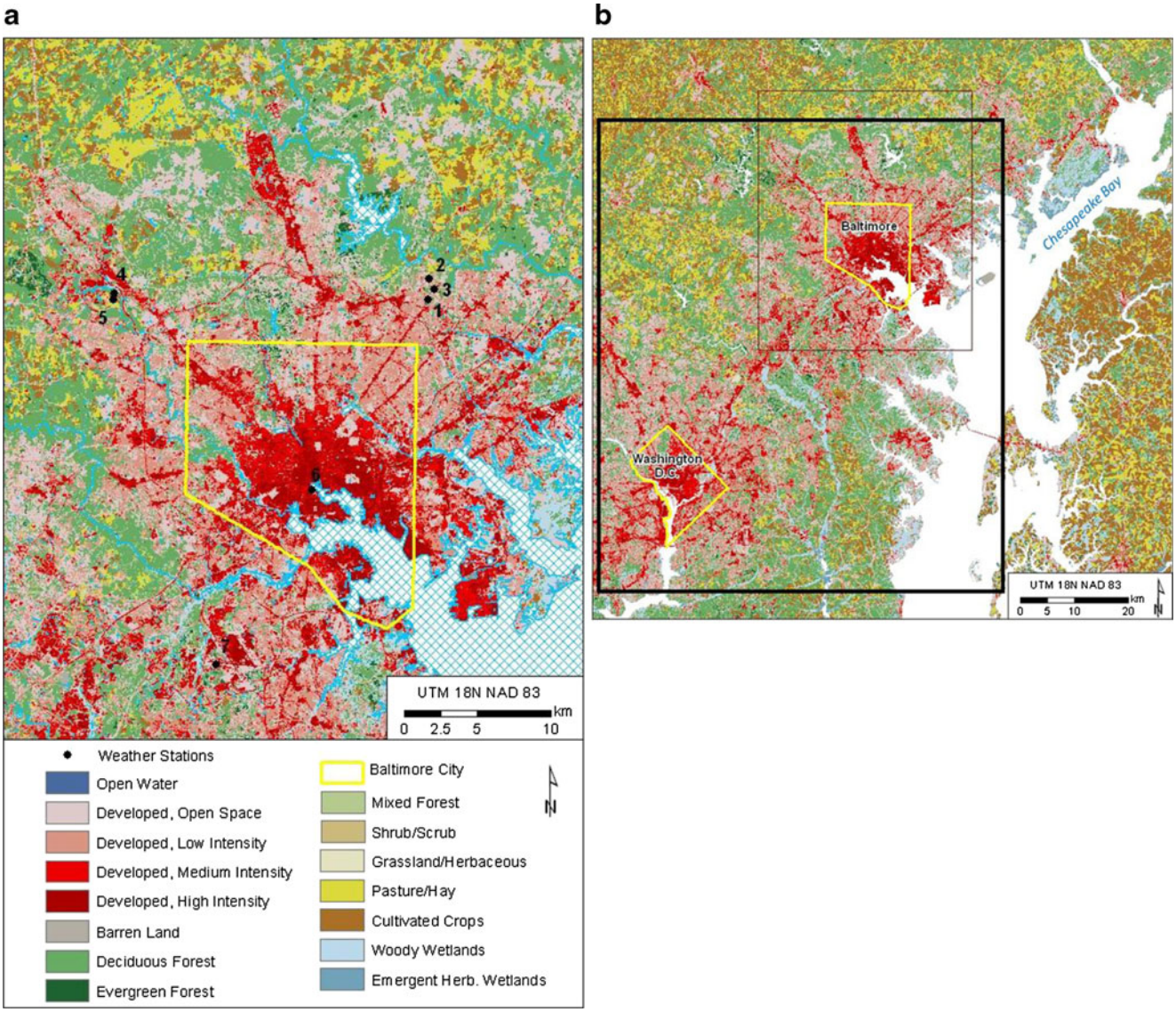

Fig. 1 **a** Land cover in the area modeled in this study, along with the location of the seven weather stations that provided data. Source of land cover: 30-m resolution 2006 National Land Cover Database (U.S. Department of the Interior 2011). **b** The location of our modeling domain (*thin black line*) within the region including the location of Washington, DC, the Chesapeake Bay, and the approximate area (*heavy black line*) of near-surface (at 2 m agl) air temperature modeling by Zhang et al (2011) shown in Fig. 8. Land cover categories are as in Fig. 1a

from solar altitude and cloud cover. The seven discrete S values range from 1 for very unstable conditions when wind is light and insolation is high during the day, to 4 for neutral stability when wind is strong or clouds prevail or when both strong wind and overcast skies are present, to 7 for very stable conditions when wind is light and the sky is clear at night. Actual atmospheric boundary layer stability varies with Earth surface roughness, which is a function of ground cover and built structure, so that actual stability in rural and urban areas at a given time are likely to differ; with more urban areas becoming less stable at night than S might indicate, because the urban structure has greater thermal entropy and remains warmer than rural areas (Panofsky and Dutton 1984). In our application, the calculated S serves as an indicator of UHI forcing, and estimating actual stability is not the object. To estimate S for each hour, we used wind speed and cloud cover from the Baltimore Washington International Airport (BWI). Cloud cover in our model domain is readily available only from the airport weather station.

Prior to modeling ΔT as a function of the full set of variables including upwind land cover, we examined the relationship between average ΔT_m and S. We looked at the difference between the means of ΔT_m in the seven different classes of S using a Tukey mean separation test (SAS Institute Inc. 2003).

2.4 Land cover

Land cover variables, tree canopy, impervious cover, and water cover were derived from LiDAR collected in 2007 and

Table 2 Characteristics of temperature sensors used in this study

Sites	Sensor	Sensor accuracy	Radiation shield	Full-sun radiation error
1, 3, 4	Model 107 thermistor, (Campbell Scientific, Logan, UT)	±0.1 °C	Model 41003 multi-plate (R.M. Young, Traverse City, MI)	<1.5 °C
2	Model 107 thermistor	±0.1 °C	Fan-aspirated, double-walled. (Designed by R.H. Grant, Purdue University)	Estimated at <0.3 °C
5	RTD (REBS: Radiation and Energy Balance Systems, Inc., Bellvue, WA)	±0.01 °C	Fan-aspirated, double-walled. (REBS)	<0.1 °C
6, 7	Platinum wire Resistive Temperature Device (RTD), (NOAA 1998)	±1 °C	ASOS Hygrothermometer	<0.6 °C

analyzed by the Spatial Analysis Laboratory (http://www.uvm.edu/rsenr/sal/index.html) at the University of Vermont using the methods of Zhou and Troy (2008). The original resolution of these data is typically 1 m. However, in this study, we modeled $\Delta \widehat{T}$ over a domain of nearly 40 by 50 km, about 1667 km^2 excluding water and a small portion outside the LiDAR coverage, and we had to aggregate the high-resolution land cover to make file sizes manageable. Thus, we re-sampled cover from the original 1-m pixel resolution to 10 m (Fig. 2).

To derive upwind land-cover differences between sites, we assumed that wind direction over the entire model domain was uniform during each hour and represented by airport wind reports. We used the uniform wind direction assumption for several reasons. The weather station at Site 6 had no wind sensors. The wind sensors at Sites 1 through 5 were at only 2 m agl, and at Sites 1 through 4, wind direction at 2 m agl was influenced by nearby trees and buildings and not likely to be representative of the general flow over and through the area. Also, one goal was to develop methodology that might be applied to other urban areas, many of which have limited sources of measured wind direction such as at an airport. The assumption of uniform wind flow over the entire area is, of course, one source of uncertainty in the modeling, because

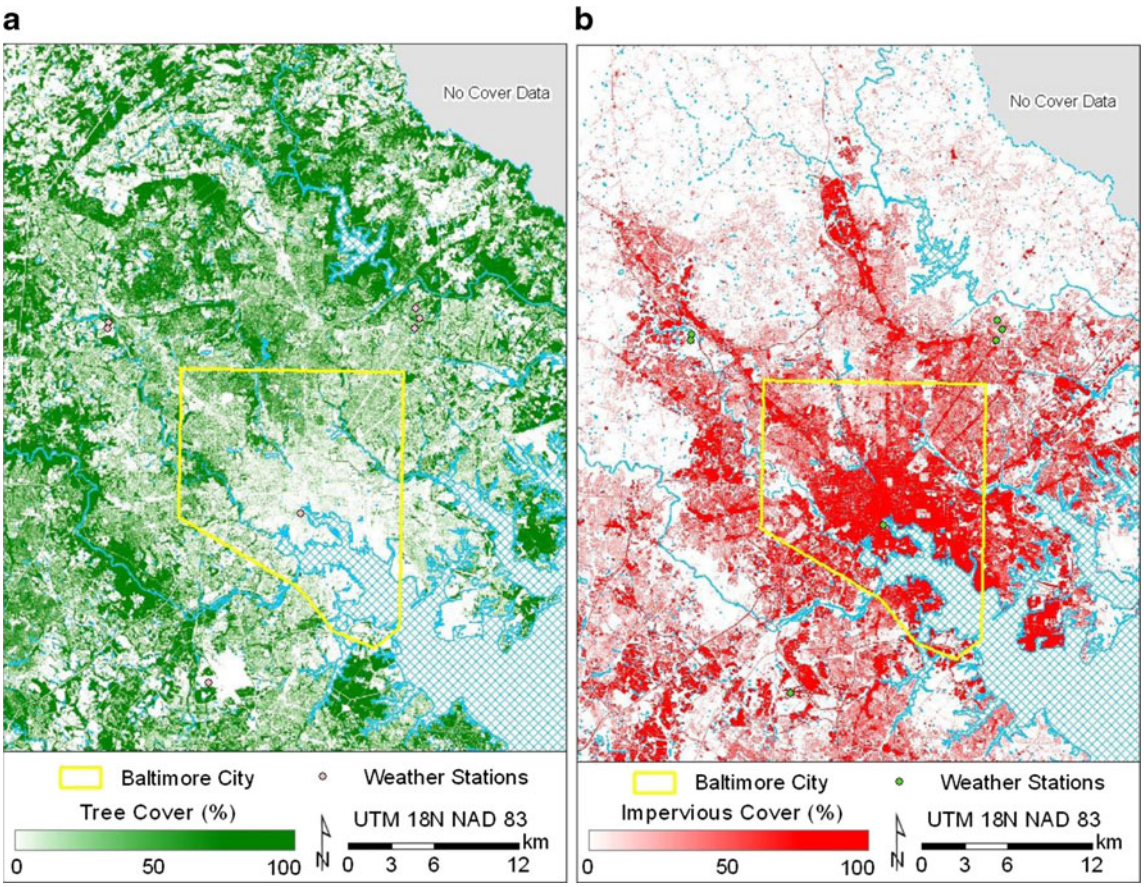

Fig. 2 **a** Tree cover in the study area derived from LiDAR analysis. **b** Impervious cover in the study area derived from LiDAR analysis

flow will differ over such a large area, especially given the potential for sea breeze (Zhang et al. 2011) and topographically induced katabatic flows (Brazel et al. 2005; Hirano et al. 2004).

A major challenge is created by the range of the spatial scales of cover influences on temperature. To create independent land cover variables, we generated an ArcGIS-based Python program to average tree, impervious, and water cover fraction over segments created by circles with 0.020, 0.0625, 0.125-, 0.250-, 0.5-, 1-, 2-, 3-, and 5-km radii centered on each of the sites, and by lines radiating from the sites to create 45° pie-shapes centered on the eight compass directions (N, NE, E, etc.), as illustrated in Fig. 3. The radii of the wedge-shaped areas for land-cover analysis were intuitively selected to provide increasing resolution for areas closer to the weather stations.

2.5 Topography

Baltimore and the suburban areas included in our study span the transition from the Atlantic Coastal Plain in the southeast of the area and the Piedmont Plateau to the northwest. The line between these physiographic provinces is known as the fall line and marks the limit of navigable waterways (http://www.mgs.md.gov/geology/). The lower elevation Coastal Plain is differentiated by the lighter areas in Fig. 4. In that figure and in our analysis, we used the USGS 2006 10-m digital elevation model (http://rmmcweb.cr.usgs.gov/elevation/dpi_dem.html). Elevation across the domain of the study ranges from sea level to 230 m. Elevations of the weather station sites range from 3 m at the Downtown Site 6 to 157 m at the Rural Open Site 5. The area includes some steep slopes, as indicated by the maximum slopes within 2 km of the weather stations (Table 1).

Topography has several influences on air temperature, including the atmospheric lapse rate and cold air drainage. The effect of average lapse rate was accounted for by elevation difference ($\Delta E_{R\text{-}s}$) as a predictor variable in the regression model, where $\Delta E_{R\text{-}s}$ is elevation at the reference site minus elevation at other sites, thus $\Delta E_{R\text{-}s}$ is negative for all six "*s*" sites.

The possible effects of cold air drainage were modeled by intuitive indices of drainage to and away from the sites. For cold air drainage away (D_{A2}) the index was defined as the product of relative elevation over 2 km around the point and absolute height above the lowest elevation within 2 km, where

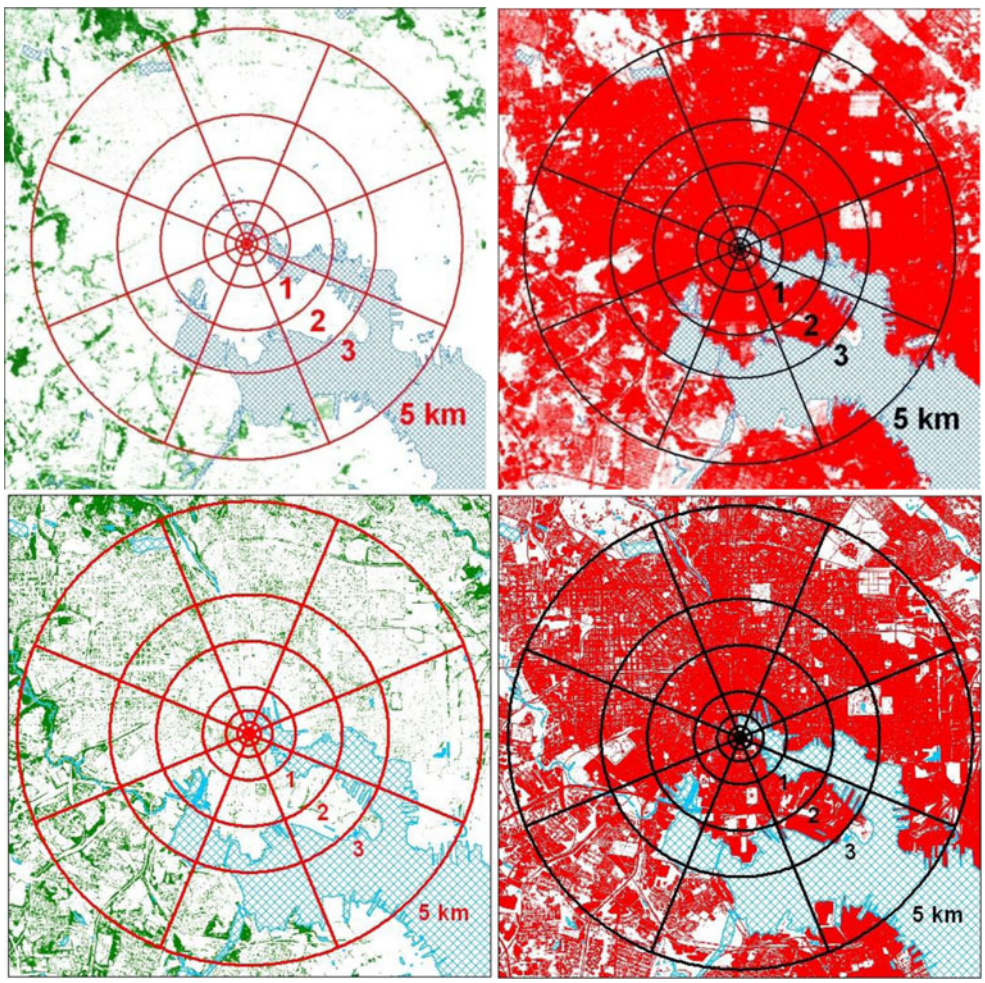

Fig. 3 Tree cover (*left*) and impervious cover (*right*) wedge patterns at the reference station in the Inner Harbor area of downtown Baltimore, from NLCD 2001 at 30-m resolution (*top*) and LiDAR-derived 10-m resolution data (*bottom*)

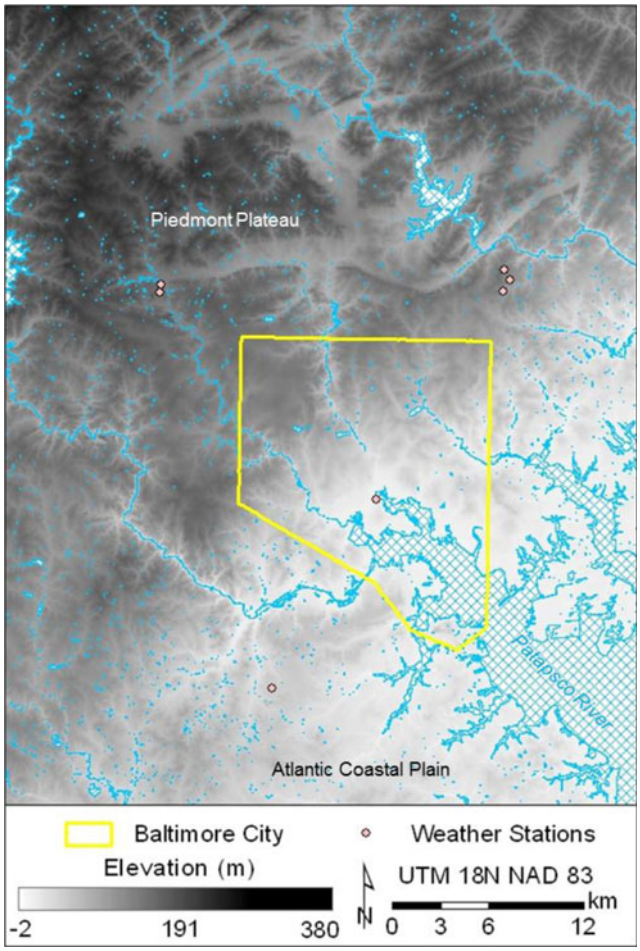

Fig. 4 Elevation over the study area from the 10-m resolution DEM available at http://ned.usgs.gov via the Seamless Data Warehouse (http://seamless.usgs.gov)

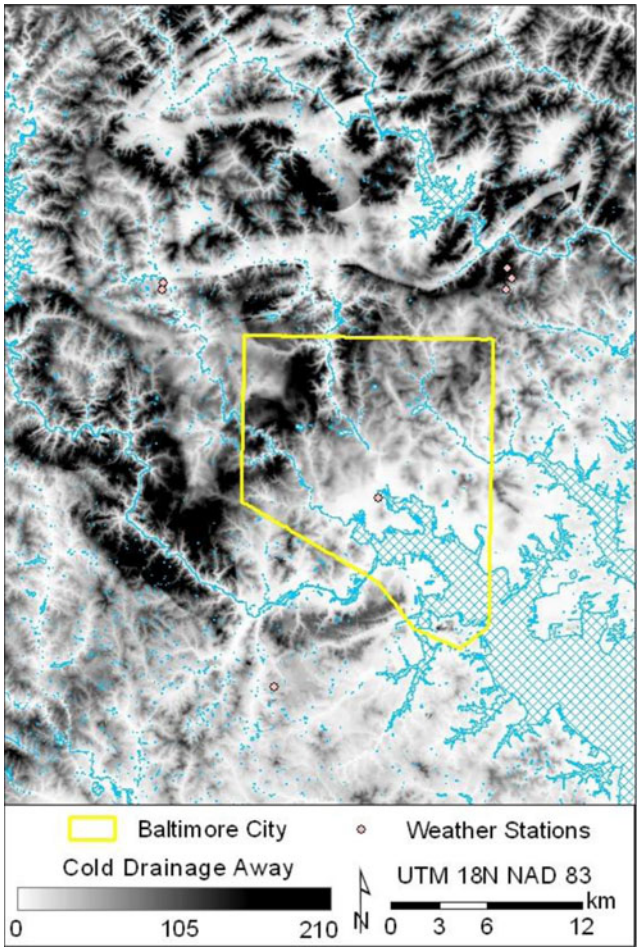

Fig. 5 Index of D_{A2}, Cold Drainage Away, at all pixels over the Baltimore ΔT modeling domain

relative elevation (E_{RL}) was the difference in elevation of the site (E_s) and the lowest elevation (E_{L2}) within 2 km, divided by the total range of elevation within 2 km (Table 1, Fig. 5).

$$D_{A2} = \frac{E_s - E_{L2}}{E_{H2} - E_{L2}}(E_s - E_{L2}) \quad (1)$$

Note in Fig. 5 that valley bottoms have low values of D_{A2}, and valley side slopes have high D_{A2}. Cold, dense air is pulled by gravity down the side slopes, but tends to settle in low-sloping valley bottoms. Similarly, for cold air drainage toward a station, an index (D_{T2}) was defined as the product of relative elevation below the highest elevation over 2 km around the point and absolute elevation below the highest elevation within 2 km (Table 1).

$$D_{T2} = \frac{E_{H2} - E_s}{E_{H2} - E_{L2}}(E_{H2} - E_s) \quad (2)$$

This simplified approach does not consider inhomogeneities in land cover, vegetation, and built features that may alter local flow patterns by turbulent friction (Brazel et al. 2005).

A related geographical feature is the Chesapeake Bay to the east and southeast of Baltimore (Fig. 1b). While the main part of the bay is nearly 20 km away from the heart of the city of Baltimore, the Patapsco River (Fig. 4) protrudes to within our modeling domain, and the Patapsco is more than 1.5 km in width well within city limits. Interaction terms of spatial water cover fraction with the temperature difference ($T_R - T_W$) between the reference station air temperature and water temperature were also tested as predictor variables. The T_W came from a National Oceanic and Atmospheric Administration buoy in the Chesapeake Bay near Baltimore. The possible influence of these water bodies on air temperature is discussed in the Results section.

2.6 Regression method

To develop a prediction equation with the temperature differences ΔT_m (that is, $T_R - T_s$, with six values each hour) as the dependent variable, we derived GIS layers of tree-cover differences, impervious-cover differences, and water-cover differences (Downtown reference–other site values) by distance

and compass direction. The cover areas for tree and impervious cover are illustrated in Fig. 3. The cover differences, for example for impervious cover, $I_{d(R\text{-}s)}$, for distance d were formed as impervious cover averaged over the 45° wind direction segment and from the coordinates of the station out to d. Thus, $I_{250m(R\text{-}s)}$ for Site 1 when wind was from an azimuth of 80° was $I_{250m(R)} - I_{250m(1)}$, where $I_{250m(R)}$ was impervious cover at the reference site over the 45° wedge between 67.5 and 112.5° and extending from the reference station out to 250 m, and $I_{250m(1)}$ was the average cover over the same shaped wedge, but with its apex at Site 1. The process was similar for tree and water cover for other wedge directions and distances. We also derived site differences for the topographic variables, elevation as $E_{R\text{-}s}$ and cold air drainage as $D_{A2(R\text{-}s)}$ and $D_{T2(R\text{-}s)}$.

We then created interaction terms of cover differences with forcing atmospheric and topographic variables. Because there are nine distances (20, 62.5, 125, 250, 500, 1000, 2000, 3000, and 5000 m) and 11 possible forcing variables (wind speed, vapor pressure deficit, cold air drainage indices, stability index, four antecedent precipitation times, elevation difference, weekend or not, and water temperature) most of which are applied as interaction terms with the three cover types, there were a total of 190 possible independent variables.

We used SAS Proc Reg (SAS Institute Inc. 2003) to derive the prediction equation for $\Delta \widehat{T}_{R\text{-}s}$. as a function of the upwind cover differences and forcing variables. This analysis rests upon the coincidence that the urban heat island intensity is approximately proportional to the S index category numbers from 1 to 7, so that a function of the index number may be used as one of the forcing variables. To select candidate predictors from among the 190 possibilities, we first used Excel spreadsheet correlation to get the correlation of all the possible independent variables with $\Delta T_{R\text{-}s}$. We then selected, from terms that were more highly correlated with $\Delta T_{R\text{-}s}$, a group that was most physically meaningful as independent variables for predicting $\Delta \widehat{T}_{R\text{-}s}$. We used the highly correlated group in stepwise regression with $\Delta T_{R\text{-}s}$ as the dependent. We did not include atmospheric forcing variables alone as independent variable candidates, but only in interactions with cover terms. In theory, if there were no cover differences, the atmospheric forcing variables antecedent precipitation, wind speed, and vapor pressure deficit would not create temperature differences. Although elevation difference is in a sense a forcing variable, it can stand alone because it is related to air temperature almost linearly because of the change in pressure with elevation. The cold air drainage index is another topographic variable, but we used it only as an interaction with stability class S because it generally becomes effective only with stable atmospheric stratification.

To sort out independent variables with high collinearity, we used the Tolerance option in Proc Reg. After the first stepwise run, we removed from the candidate variable list those that were not significant. If any Tolerance values were less than 0.4, we also removed the one with the lowest Tolerance from the candidate list. We then reran the stepwise, repeating the process until all variables had a Tolerance value of at least 0.40. Though there is no strict rule for minimum acceptable tolerance, Allison (1999) suggested that tolerance should be at least 0.40 to avoid excessive multicollinearity.

2.7 Mapping temperature differences

We produced hourly maps of predicted temperature difference, $\Delta \widehat{T}_{R\text{-}p}$ with ArcGIS. This required using the regression prediction equation to calculate $\Delta \widehat{T}_{R\text{-}p}$ for each 1/3 arc second (or 10×10-m pixel) in the modeling domain, that is for each point p. We mapped layers of tree canopy and impervious cover differences from reference site values, again pixel by pixel, for each of the eight wind directions and significant distances in the prediction equation. Similarly, we created layers of indices of cold air drainage differences, $D_{A2(R\text{-}p)} = D_{A2(R)} - D_{A2(p)}$, where $D_{A2(R)}$ is cold air drainage index at the reference location, Site 6, and $D_{A2(p)}$ is the index at each 10-m pixel. We then used the cover and cold air-drainage difference layers along with airport weather data and S Class to map $\Delta \widehat{T}_{R\text{-}p}$ across the domain. We then modified the maps of $\Delta \widehat{T}_{R\text{-}p}$ to have a temperature scale ranging from 0 for the warmest pixel on the map to negative values that ranged up to the temperature of the coolest pixel on the map.

3 Results

There were 3528 hours between May 5, 2006 and September 30, 2006, but the measurements of air temperature were simultaneously complete at all seven of our sites for just 1681 of those hours. There were six temperature differences (reference site–each of the other sites each hour, $\Delta T_{m(R\text{-}s)}$), thus there were a total of 10086 observations of $\Delta T_{m(R\text{-}s)}$. Most commonly, it was the ASOS sites with missing data. The number of observations varied by S from 234 in S 1 to 3204 in S 4 (Table 3).

3.1 Dependence of ΔT_m on stability class

For the seven Baltimore stations, mean $\Delta T_{m(R\text{-}s)}$ generally increased with S (Fig. 6, Table 3), though not monotonically. Very unstable S 1, which occurs with low wind speed, clear skies, and high solar elevations, had the lowest mean $\Delta T_{m(R\text{-}s)}$. Stability Class S 1 occurs in midday when the sky is clear and wind speed is relatively low. The small $\Delta T_{m(R\text{-}s)}$ with S 1 occurs in part because urban surfaces are slower than rural surfaces to warm after the large nighttime temperature differences (Oke 1987). The $\Delta T_{m(R\text{-}s)}$ is also small with S 1 because vertical convection mixes air aloft with air near the Earth surface, thus tending to equalize temperatures across the landscape.

Table 3 Mean $\Delta T_{m(R-s)}$ and standard error (SE) by stability class, significant differences of mean $\Delta T_{m(R-s)}$ determined by a Tukey's HSD mean separation test (shown by different letters in the Significance column, with means having different letters being significantly different)

Stability class	Stability description	Number	Mean ΔT_m and SE	Significance
7	Very stable	1362	4.27±0.048	a
6	Moderately stable	1554	3.75±0.046	b
5	Slightly stable	696	2.84±0.057	c
3	Slightly unstable	1878	2.54±0.037	d
2	Moderately unstable	1158	2.31±0.046	de
4	Neutral	3204	2.13±0.023	ef
1	Very unstable	234	1.99±0.095	f

With neutral stability, S 4, mean $\Delta T_{m(R-s)}$ was slightly higher than with S 1 but the difference was not statistically significant (Table 3). Moderately unstable S 2 had higher mean $\Delta T_{m(R-s)}$ than S 1, and the difference was statistically significant. At the highest stability, S 7, the mean temperature difference was more than double that of the least stable.

3.2 Prediction equation for $\Delta \widehat{T}$

The regression analysis resulted in an equation for $\Delta \widehat{T}_{R-s}$ that uses a total of 14 variables, combined into 10 predictor terms, 9 of which are multiplicative interactions (Table 4). The adjusted R^2 of 0.50 indicates the equation explains about 50 % of the variance in the $\Delta \widehat{T}_{R-s}$. Variables are defined in Table 5. The form of the model in Table 4 is:

$$\Delta \widehat{T}_{R-s} = 0.669 + 0.00851\left(I_{250m(R-s)} \bullet (S_3)^3\right) - 0.00252\left(I_{500m(R-s)} \bullet \mathrm{End}\right) + \ldots + 0.00945(E_{R-s}) \quad (3)$$

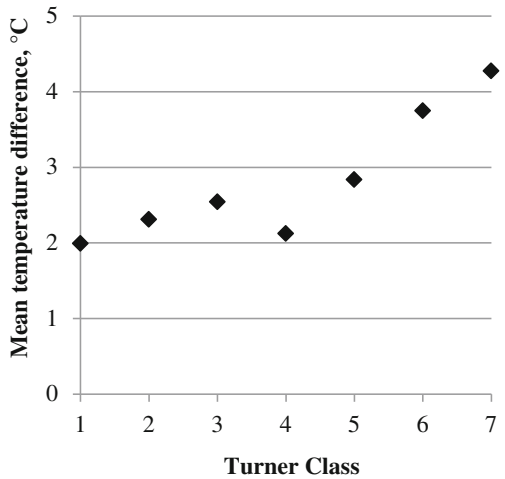

Fig. 6 Mean $\Delta T_{m(R-s)}$. by Turner Class. Significant differences among $\Delta T_{m(R-s)}$.shown in Table 3

Table 4 Regression equation for $\Delta \widehat{T}_{R-s}$, given all stability classes, n= 10,086, R^2=0.50, 10 significant terms with α=0.05, and a total of 14 variables according to variable definitions in Table 5

Cover or topographic variables	Atmosphere interaction terms		β	Tolerance
		Intercept	0.670	
$I_{250m(R-s)}$	$(S_3)^3$		0.00851	0.43
$I_{500m(R-s)}$	End		−0.00252	0.96
$I_{5k(R-s)}$	$(S_3)^3$		0.0166	0.40
$t_{125m(R-s)}$	$(S_3)^3$		−0.00316	0.41
$I_{62m(R-s)}$	$U_{/100}$		−0.0912	0.59
$I_{250m(R-s)}$	U_I		0.00853	0.41
$t_{20m(R-s)}$	VPD		−0.00676	0.83
$D_{A2(R-s)}$	$(S_3)^3$		−0.0112	0.53
$I_{20m(R-s)}$	Rain		0.00488	0.67
E_{R-s}			−0.00945	0.82

The predictor variables include upwind tree cover and impervious cover differences, interactions with S, a weekend versus weekday indicator, airport wind speed and vapor pressure deficit (VPD), an index of likely cold air drainage away from the site, rainfall within the last hour, and elevation difference from the reference station. Significant upwind impervious cover differences extended from 20 m up to 5 km, whereas significant tree canopy cover differences extended from only 20 to 125 m. This does not suggest that tree cover has an influence over only a distance of 125 m; tree cover is inversely correlated with impervious cover. Moreover, in the land-cover analysis, where tree canopy was over impervious cover, that area was counted as tree.

The model in Table 4 has an intercept of about 0.67. An intercept can be viewed as the result of variability in the measurements that is not accounted for by cover, topography, or atmospheric forcing variables. In prior modeling for the summer of 2004, Heisler et al. (2007) finished by running the regressions a final time with the No Intercept option. We have not done that in this analysis, partly because the intercept was sufficiently small that it would have little practical significance (and because with No Intercept, the coefficient of determination, R^2, loses meaning).

Interpretation of the influences of the predictor variables in Table 4 necessitates remembering that the cover and topographic variables are differences, reference site – others. Because the reference point, Site 6, had high impervious cover and low tree cover, the impervious cover differences ($I_{250m(R-s)}$, $I_{500m(R-s)}$, etc.) were usually positive, and tree cover differences ($t_{20m(R-s)}$, $t_{125m(R-s)}$) were usually negative. If a point s away from the reference had a lower value of $I_{250m(R-s)}$ than the reference, then $I_{250m(R-s)}$ at s would be positive, and the positive β and $(S_3)^3$ would indicate a positive influence on $\Delta \widehat{T}$, which

Table 5 Definition of variables

Variable[a]	Variable definition
$D_{A2(R-s)}$	Cold Drainage Away, Within 2 km, (elevation−lowest)^2/(highest−lowest)
E_{R-s}	Elevation at reference weather station–elevation at other weather station
End	Weekend=1, weekday=0
$I_{20m(R-s)}$	Difference in impervious cover, 0 to 20 m upwind, Site 6–other sites
$I_{250m(R-s)}$	Difference in impervious cover, 0 to 250 m upwind, Site 6–other sites
$I_{500m(R-s)}$	Difference in impervious cover, 0 to 500 m upwind, Site 6–other sites
$I_{5k(R-s)}$	Difference in impervious cover, 0 to 5 km upwind, Site 6–other sites
$I_{62m(R-s)}$	Difference in impervious cover, 0 to 62 m upwind, Site 6–other sites
U_I	1/wind speed (m s^{-1}) with wind speed set to 1 if reported as 0
$U_{/100}$	Wind speed (m s^{-1})/100 with wind speed set to 1 if reported as 0
Rain	1/((Current hour rainfall in inches)×100+1)[b]
$t_{125m(R-s)}$	Difference in tree canopy cover, 0 to 125 m upwind, Site 6–other sites
$t_{20m(R-s)}$	Difference in tree canopy cover, 0 to 20 m upwind, Site 6–other sites
$(S_3)^3$	The cube of Turner Class stability index averaged over the last 3 h[c]
VPD	Vapor pressure deficit, mb

[a] The subscript *(R-s)* indicates difference between the reference site, *R*, and other weather stations, *s*

[b] Precipitation in the USA is commonly reported in inches, 1 in.= 25.4 mm

[c] The capital full-size *S* represents stability index

equates to cooler temperature at *s*. The same rationale applies to the $I_{5k(R-s)}$•$(S_3)^3$ term. The interaction for tree cover over 125 m and stability, $t_{125m(R-s)}$•$(S_3)^3$, has a negative β indicating an increase in $\Delta\,\widehat{T}$ (cooler temperature) as tree cover increases at point *s*. Similarly, for the tree cover interaction with vapor pressure, $t_{20m(R-s)}$•VPD, with greater VPD, the dryer air will increase evapotranspirational cooling from tree cover, and the combination of greater tree cover at *s* and higher VPD will lead to a larger magnitude negative that, with the negative β, will increase $\Delta\,\widehat{T}$, meaning cooler temperature at *s*.

On weekdays, measured temperature differences between the reference site and other sites averaged about 0.18 °C greater than on weekends, that is, the reference site was relatively warm. The difference in means was statistically significant. This effect may be caused by the fact that the reference site is the most urbanized, and its greater density of transportation and industrial heat sources may lead to higher temperature on week days. The weekend effect was included in the model by the $I_{500m(R-s)}$•End interaction, where End=0 on weekdays and 1 on weekends. The sign of the β in Table 4 indicates that at points with lower impervious cover than the reference point ($I_{500m(R-s)}$ positive), predicted $\Delta\,\widehat{T}$ will be more negative, that is, temperatures at points with low impervious cover will be relatively cooler on weekends compared to weekdays. The 500 m of upwind impervious cover difference is an intuitive estimate of a significant extent of impervious cover that would produce significant anthropogenic emissions.

The two terms containing interactions with impervious cover and wind speed counteract or combine with other variables that include impervious cover. The $I_{62m(R-s)}$•$U_{/100}$ term with its β of −0.091 reduces $\Delta\,\widehat{T}$ (makes a point *s* with low $I_{62m(R-s)}$ warmer), but the reduction is larger as wind speed increases. This counteracts the effect of increased $\Delta\,\widehat{T}$ in other terms with low impervious cover. In the U_I interaction with $I_{250m(R-s)}$, a point *s* with low $I_{250m(R-s)}$ has increased $\Delta\,\widehat{T}$ when wind speed is low, but as wind speed increases, the term becomes smaller.

Table 4 includes no term for water cover effects, despite the presence of significant water area within the modeling domain (Fig. 1). In a previous analysis with separate regression analysis for each *S* (Ellis 2009; Heisler et al. 2007), an interaction term for water cover and the difference in temperature between air and water temperature did appear as significant for *S* classes 2 and 6. Part of the reason for water cover not appearing in the current analysis is that the large areas of Chesapeake Bay are to the southeast, a direction little represented in the general wind climatology for the area. Furthermore, our modeling domain is sufficiently far from the main part of the Bay that the weather stations may be generally beyond a classic daytime bay breeze influence, although the bay breeze effect requires further study. Zhang et al (2011) did find a bay breeze effect on temperature and a bay breeze shift in wind in their mesoscale modeling of temperatures in the Baltimore Washington metropolitan area for mid-afternoon on July 8 and 9, 2007 (see section 3.3 below). The wind shift extended from the main portion of the bay nearly, but probably not quite, to our Sites 6 and 7 (Downtown and airport).

Sikora et al. (2010) pointed out that bay breezes extend relatively shorter distances inland from the western shore of the Chesapeake than water body breezes from larger bodies of water, such as Lake Michigan. They detected bay breezes at the BWI airport, about 23 km from the bay, on 7, 12, 10, 12, and 9 % of the days in the months of May, June, July, August, and September, respectively, from 2001 through 2005. On the days when bay breezes extended as far as the BWI airport, our model would have at least somewhat reflected the bay breeze influence, because the assumed wind direction over our modeling domain is based on the airport data. However, bay breeze frequency is greater closer to the bay; for example at an ASOS station to the northeast of our model domain and just

2 km inland, bay breezes were found on 25 % of the days in June (Sikora et al. 2010).

In general, regression modeling has the potential for arriving at a large range of somewhat different models and requires use of considerable judgment regarding the physical processes at work (Burnham and Anderson 2002). For example, in our stepwise regression, $E_{R\text{-}s}$ was initially not selected as a significant variable. Physically, an elevation difference coefficient of about 0.01 is expected in order to account for the average atmospheric lapse of about 0.01 °C/m. Therefore, we added $E_{R\text{-}s}$ as an additional variable after the stepwise regression was complete, and it was then significant and had a Tolerance >0.40.

A possible alternative to a regression model that includes the data for all of the stability classes together would be to do separate analyses and produce separate regressions for each of the seven S classes. One reason for analysis by separate S classes is that for studies of the effect of tree cover and temperature on air quality, the unstable classes occurring in daytime with warmer temperatures will be of most interest. Because neutral stability, S 4, has more hours of observation than unstable Classes 1, 2, and 3, a model of all classes combined may be weighted away from the unstable classes. Bay breeze effects may also be more easily captured in models that include the unstable daytime classes individually.

Initial analysis of the regression residuals, $\Delta T_{R\text{-}s} - \Delta \widehat{T}_{R\text{-}s}$, measured minus predicted values of the dependent variable, suggested that further exploration would lead to model improvements. At some sites, in times of early morning transition, residuals were large, apparently because the 3-h average of S is too long to adjust to the rapid change in solar input. The additional analysis of model residuals could examine whether large residuals occur for particular stations, times of day, or stability indices.

Larger residuals may also have occurred at times of frontal passage across the domain. In a study of UHI effects in Lodz, Fortuniak et al. (2006) excluded data during times when frontal systems moved across the city. For our Baltimore study, we excluded hours of data from all stations only if one or more of the sites had missing temperature values.

3.3 Mapping $\Delta \widehat{T}$

Using the airport weather data to represent synoptic conditions, we mapped the Eq. 3 (Table 4) model across the Baltimore region for individual hours. For each pixel in the domain, upwind land cover and topographic differences from the reference Site 6 were determined so that $\Delta \widehat{T}_{R\text{-}p}$ could be derived from Eq. 3 for each point p in the domain. That is, the subscripts of $\Delta \widehat{T}$ and the land cover values became $_{R\text{-}p}$ rather than $_{R\text{-}s}$. To somewhat enhance viewing the pattern, we adjusted the $\Delta \widehat{T}_{R\text{-}p}$ maps to create images with the warmest location on the map having a temperature difference, $\Delta \widehat{T}_{rel}$, of 0, and all other pixels having negative $\Delta \widehat{T}_{rel}$. This yielded results as illustrated in Fig. 7. The times for these illustrations were selected for having as little ambiguity in thermal stability conditions as possible; in that S was unchanged for at least 3 h. In Fig. 7a, c represent times of relatively clear skies, conditions in which S 1 and 7 occur. Figure 7b shows an S 4 example with low wind speed at midday with cloudy skies. Maps for all S (Turner Class) values are included in Online Resource 1.

By removing the $\Delta E_{R\text{-}s}$ and $D_{A2(R\text{-}s)} \bullet (S_3)^3$ terms from the model, the topographic influence is removed, leaving only impervious cover and tree canopy cover effects on $\Delta \widehat{T}$. Figure 7d illustrates a map without elevation influence for S 7 conditions. On the Coastal Plain where relief is small, there is little difference from the case with elevation, Fig. 7c. Differences are larger in the higher elevation in the northern part of the region. The maps in Online Resource 1 include examples with and without elevation for all S's.

We evaluated heat island intensity, $maxT_{u\text{-}r}$, as the difference between the warmest and coolest pixels on each hourly map. These are noted near the upper right corner in each of the map labels in Fig. 7, and for representatives of all S's in Table 6. With topographic terms in the model, $maxT_{u\text{-}r}$ ranged from 4.4 for S 2 to 12.4 °C for S 7. With topographic terms removed, $2.3 < maxT_{u\text{-}r} < 10.5$ °C. For S 6 and S 7, the warmest locations turned out to be in Developed Open Spaces, which were large stone quarries that had dense impervious surfaces.

In most studies, the rural location for determining $\mathrm{maxT_{u\text{-}r}}$ represents an agricultural area, and thus $maxT_{u\text{-}r}$ does not approximate simply a difference caused by human impact; because both urban and rural sites are strongly human influenced. The $\Delta \widehat{T}$ maps could permit estimation of a $maxT_{u\text{-}r}$ that would be more representative of human influences on temperature by evaluating $maxT_{u\text{-}r}$ with a forested rural reference that would approximate conditions before major human encroachment. The examples in the Fig. 7 legends represent merely the largest $maxT_{u\text{-}r}$ on the maps, without specific selection of the rural land use, though most of the cool rural land uses were deciduous forest. This is illustrated in Table 6, which lists examples of $maxT_{u\text{-}r}$ for each of the seven S classes along with the land uses in which the coolest and warmest points were located.

Depending upon the general climate, recent precipitation patterns, and particular land uses, we would expect that for very stable night conditions, air over open spaces with short vegetation would be cooler than air below a forest canopy (at 1.5 m, as in our data). Our results in Table 6 for S=7 indicate forests were predicted to be coolest. All of the Table 6 examples were taken from mid-September, and the especially cool forests may have been caused by soils in open areas being still moist from precipitation early in September, which could have resulted in high thermal admittance that affected temperatures

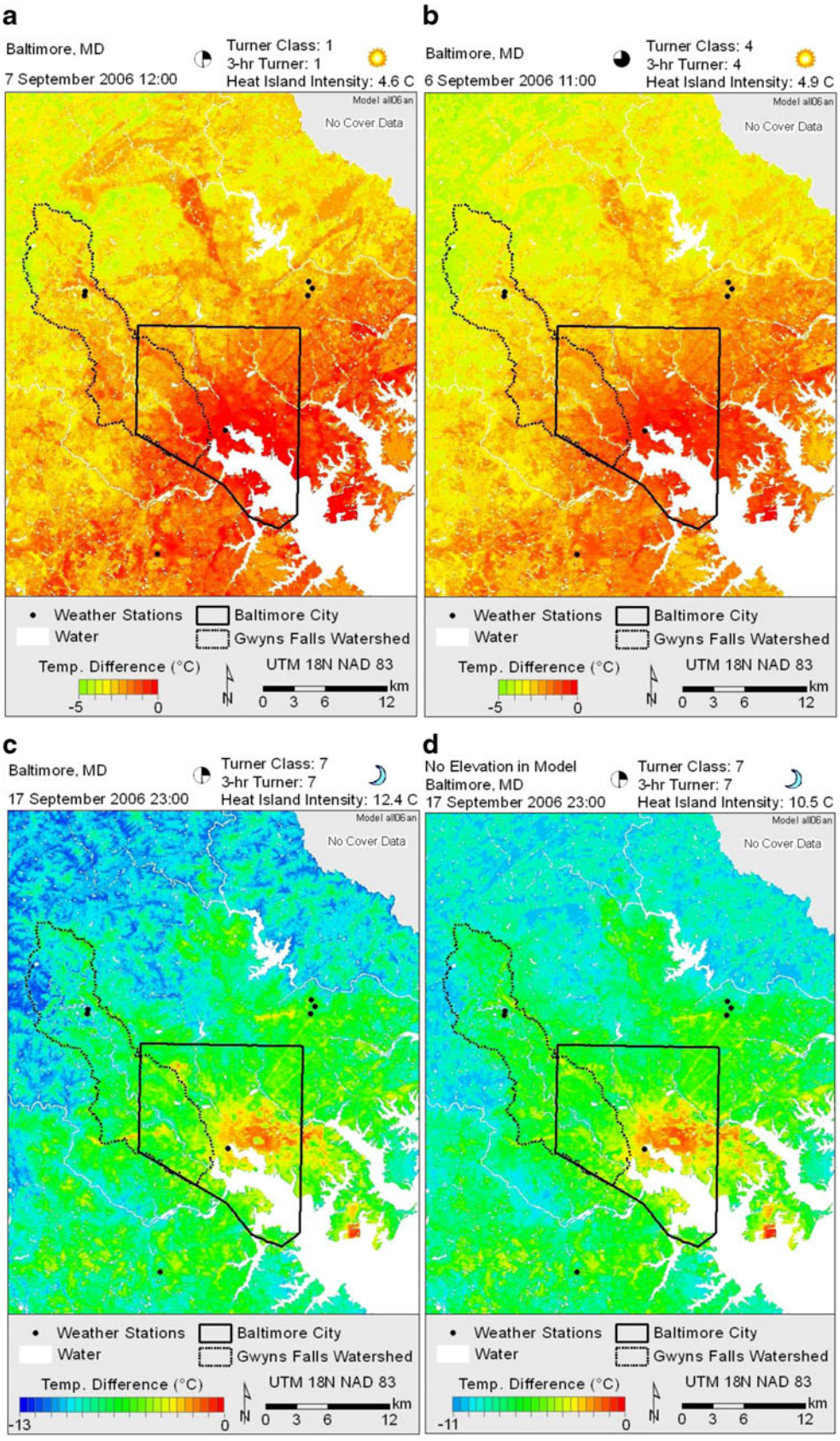

Fig. 7 **a** Example of mapped predicted temperature difference, $\Delta\widehat{T}_{rel}$ (the warmest map location having $\Delta\widehat{T}_{rel}=0$), with $S=1$ over the last 3 hours, in this case for 12:00 noon, on September 7. **b** Example of mapped $\Delta\widehat{T}_{rel}$, 11:00 on September 6, with $S=4$ over the last 3 h. **c** Example of mapped $\Delta\widehat{T}_{rel}$, 23:00 on September 17, with $S=7$ over the last 3 h**. d** Example of mapped $\Delta\widehat{T}_{rel}$, 23:00 on September 17, with $S=7$ over the last 3 h, but with no elevation terms in the equation

Table 6 Maximum heat island intensity by *S* with and without elevation in the model and land covers (as depicted in Fig. 1) of maximum and minimum temperatures without elevation in model, from maps of $\Delta \widehat{T}_{rel}$ in Online Resource 1

Turner class, *S*	$MaxT_{u\text{-}r}$ with elevation, °C	$MaxT_{u\text{-}r}$, no elevation, °C	Elevation effect on $Max\ T_{u\text{-}r}$, °C	Coolest, warmest land uses	
				Coolest	Warmest
1	4.6	2.3	2.3	Forest	High intensity develop
2	4.4	2.3	2.1	Dev. open[a]	High intensity dev.
3	4.8	2.8	2.0	Forest	Medium intensity dev.
4	4.9	3.1	1.8	Forest	High intensity develop
5	6.1	4.6	1.5	Forest	High intensity develop
6	8.0	6.5	1.5	Forest	Medium intensity dev
7	12.4	10.5	1.9	Forest	Medium intensity dev.

[a] Park land

over open more than in forests. This is an area for additional investigation.

For planning purposes, political or specific topographic areas may be of interest. Mapping of $\Delta \widehat{T}$ could permit such analyses. For example, Fig. 7 maps include the boundary of the City of Baltimore and of a topographic feature, the Gwynns Falls Watershed, which has been used as a planning unit in the Baltimore region and which is a focal point for the Baltimore Long Term Ecosystem Study (http://www.beslter.org/). Also, temperatures of large urban parks can become evident. For example, in Fig. 7c, d, the cool rectangle near the center of the city is the 56-ha Patterson Park.

3.4 Comparison to mesoscale model

Our empirical results can be compared to the pattern of air temperature using the Weather Research and Forecast (WRF) mesoscale model combined with a single-layer urban canopy model[1] by Zhang et al. (2011). They predicted 2-m agl temperatures at 15:30 on July 8 and July 9, 2007 for the Baltimore and Washington metropolis as shown in Figs. 1b and 8. Our domain overlapped part of theirs. We used the weather data from July 8 and 9, 2007 at 15:00 and 16:00 LST along with Eq. 3 to create maps of predicted temperature, which we then averaged to create Fig. 9, which is comparable in time to Fig. 8 adapted from Zhang et al. Note that Fig. 9 shows actual temperature rather than ΔT as in Fig. 7.

[1] The numerical model used by Zhang et al. (2011)is a two-way interactive, "quadruply" nested version of the Weather Research and Forecast (WRF-V2.2) model, coupled with a single-layer urban canopy model with a finest grid size of 0.5 km (Chen et al. 2010). Zhang et al. found generally good agreement of the spatial pattern of their simulated ground surface temperatures (T_{SKIN}) with observations of T_{SKIN} by MODIS satellite measurements at 1840 UTC July 8 and 1745 UTC July 9, 2007. Reasonable agreement was also found between simulated air temperature 2 m agl at four ASOS stations (BWI, Aberdeen Proving Grounds, downtown Baltimore, and Washington National Airport) and the 1.5-m height temperature measurements there. Similar comparisons were made for wind.

The general pattern of temperatures in the overlapping domains of Zhang et al (Fig. 8) and this study (Fig. 9) are remarkably similar within the limitation of the resolution, partly because of the larger area included, in Fig. 8. On July 9, Fig. 8 shows cooling along the eastern edge because of modeled bay breeze while in Fig. 9 that area is about 1.5 to 2.0 °C warmer. On July 8, wind direction at the BWI airport was from 270 and 250° at 15:00 and 16:00, so for these hours our model runs assumed upwind cover in the 45° segment centered on west (W) over the entire domain. The corresponding BWI wind directions on July 9 were 230 and 250°, so we averaged maps that assumed upwind cover in the SW and W 45° segments. For July 8, the wind vectors are also from W over the entire area of our domain in Fig. 8, which matches our assumption. On July 9, our assumption of SW to W wind direction matches Fig. 8 over the northeastern half of our domain, but the wind vectors on the eastern and southern edges of our domain in Fig. 8 are predicted to be decidedly S to SE because of bay breeze.

The bay breeze on July 9 may have been unusually strong because of the unusually high temperatures over land. In general, bay breezes may be relatively minimal compared to other land locations near large bodies of water because in the relatively shallow bay, water temperatures are rather warm. The NOAA Interpretive Buoy System (buoybay.noaa.gov) measures bay water temperatures, including at a buoy near Baltimore called Patapsco. There, peak water temperatures in mid-afternoon in July 2007 frequently exceeded 27 °C and reached as high as 30.1 °C.

Maximum and minimum temperatures over our domain agree closely with those of Zhang et al. (2011). Our maximum temperatures were 34.7 and 36.1 °C on July 8 and 9, respectively, which compares to 34.0 and 36.0 °C as best one can extrapolate from Fig. 8. Our minimum temperatures were 31.2 and 32.7 °C, which compares to about 29.0 and 32.0 °C in the area of our domain in Fig. 8. The elevation of up to about 230 m explains part of the reason for cooler temperatures in the northwest corner of our domain. The $E_{R\text{-}s}$ coefficient of −0.00945 °C/m indicates a $\Delta \widehat{T}_{R\text{-}s}$ of 2.2 °C,

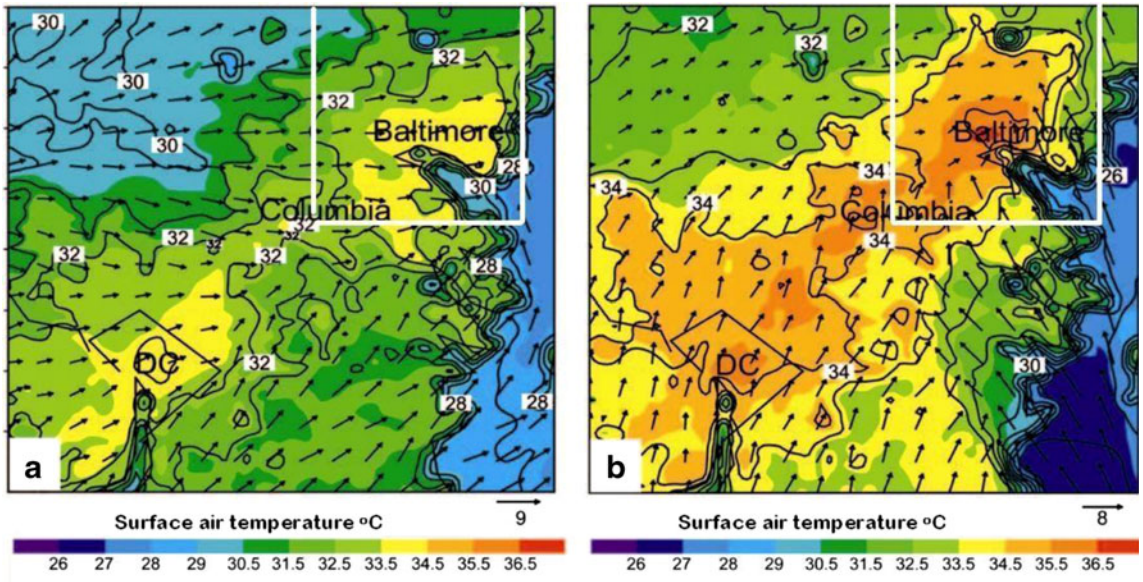

Fig. 8 Distribution of 2-m agl air temperature (°C) shown by shading, wind vectors (scale shown by vectors), contours of potential temperature for **a** July 8, 2007 at 15:30 LST and **b** July 9, 2007 at 15:30 LST by Zhang et al (2011); and the approximate domain (*white lines*) of our empirical model temperatures as shown in Fig. 9 [Figure adapted from Zhang et al. (2011) ©American Meteorological Society. Used with permission.]

which means that more than half of the temperature range of 3.5 and 3.4 °C on July 8 and 9 in our model results was owing to elevation differences. Extrapolation from Fig. 8 suggests a range of about 5 and 4 °C within our domain area in the Zhang et al. study. Thus, our results indicate a smaller UHI by 1.5 and 0.6 °C, but not significantly smaller maximum temperatures.

A primary conclusion of Zhang et al. (2011) was that the Baltimore UHI is influenced by upwind development as distant as Washington, DC, about 60 km SW of Baltimore, and that the long-range advection added about 1.5 °C to the Baltimore UHI. In contrast, the most distant cover considered in Eq. 3 is only 5 km. Because our model results begin with a T_R that is fortuitously close to the warmest point in Baltimore,

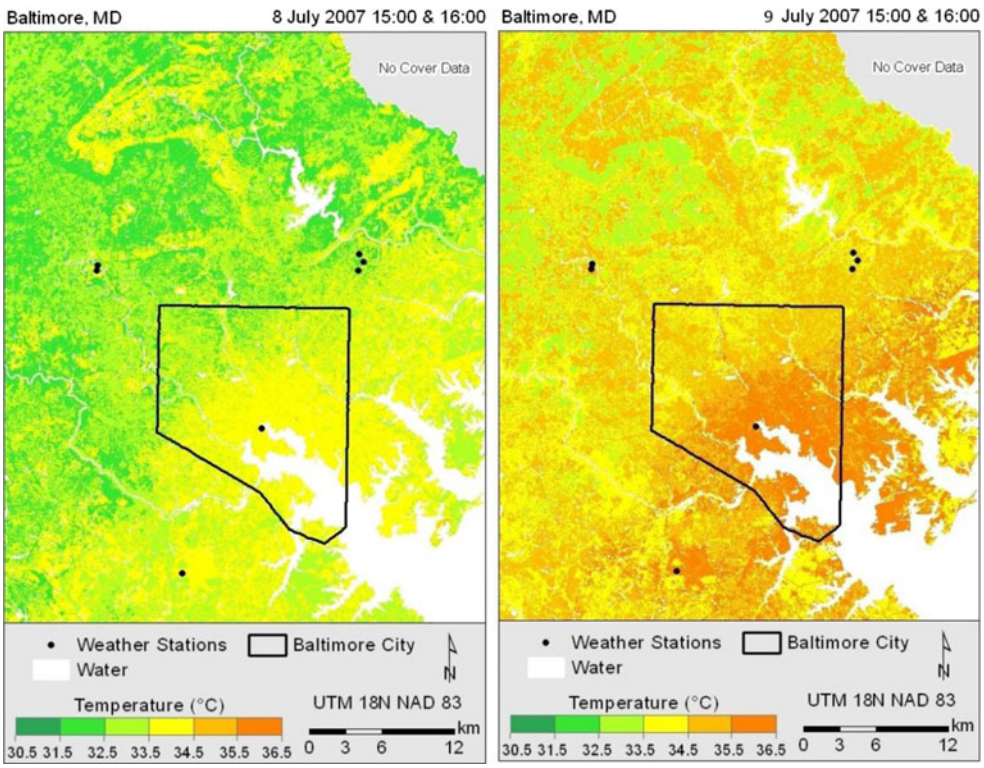

Fig. 9 Our model runs corresponding to the times modeled by Zhang et al. (2011), 15:30 on July 8 (*left*) and July 9 (*right*)

as indicated by both models, our maximum temperatures are likely to be realistic. On the other hand, if 1.5 °C is routinely added by long-range advection to the daytime UHI across the city, it would be significant for many issues of environmental concern and something that a model based on up to only 5 km of upwind cover could not predict. However, the conditions of July 9, including the very high temperatures, are somewhat uncommon.

4 Discussion

The modeling method used here accounts for most of the hypothesized causes of urban climate disparity from rural climate (see section 1), but in some respects the accounting is indirect rather than explicit. For example, anthropogenic heat emissions from transportation occur over impervious cover and likewise buildings are impervious cover and thus percent impervious cover is related to anthropogenic heat release. Similarly, daytime heat storage and nighttime release are related to thermal admittance (Oke et al. 1991; Runnalls and Oke 2000), which is high for impervious cover and usually low for pervious cover. Thermal admittance of soil is increased by increases in soil moisture (Oke et al. 1991), which especially increases average thermal admittance of rural areas, thus reducing urban to rural contrast and the UHI effect. Difference in soil moisture is accounted for in our model by the term for antecedent precipitation. Less well accounted for is the difference in sky view caused by tall building. In future modeling, this lack could be largely corrected by using LiDAR data to estimate shortwave radiation penetration (Lindberg and Grimmond 2011). The LiDAR data include building and tree height, which can be combined with the building cover and tree cover to estimate average building and tree volume per pixel for use as predictor variables that should be more closely related to sensible heat flux.

LiDAR data are becoming increasingly available. For example, in addition to LiDAR coverage for all of Baltimore County, Maryland and two adjacent counties, LiDAR coverage was recently provided for the city of Syracuse, NY and analysis of LiDAR data are ongoing for New York City. Thus, analyses similar to the one reported here may be possible in many more cities. The extent to which empirical models developed for one city may apply to others remains to be tested. A major concern is that the range of cover and topographic variables will differ from city to city, so that in applying a model from a different city, extrapolation beyond the range of independent variables used in developing the model may be required, resulting in erroneous results.

We expect that high-resolution cover data, such as the 10-m data used here are better able to account for small-scale structure, such as individual or small groups of trees. Our previous analyses (Ellis 2009; Heisler et al. 2007) used 30-m resolution National Land Cover Database (NLCD) (http://www.mrlc.gov/nlcd01_data.php) cover. With the lower resolution, the shortest distance over which cover could be averaged for creating independent variables was 125 rather than 20 m. The NLCD is known to significantly underpredict both tree cover and impervious cover (Greenfield et al. 2009). The difference between tree cover and impervious cover in NLCD and our high-resolution cover is obvious in Fig. 3. The cover averaging did smooth over most of the detail in our 10-m resolution cover. By including differences in average cover over 20 and 62.5 m around the stations, the finer 10-m cover resolution seemed to improve explanatory power as indicated by increased R^2, but further comparison of results with NLCD and high-resolution cover for identical spatial domains and weather data are needed.

A number of additional steps could be carried out in future analyses. Some of these include:

1. Include cover volume differences for tree and building land use, where volume is average cover times average height.
2. Check modeling results with other weather data. One possibility is the use of data from the Weatherbug school weather station network or Weather Underground data. These stations will probably have some differences from the data used here, because most of the stations are above school roofs, rather than near the ground at 1.5 m height.
3. Run regressions for winter periods. For some applications, like influences of trees on heating and cooling buildings, the all-year influence is important.
4. Compare model results for all stability classes combined, as in this study, to results of modeling individual stability classes separately. A single model is somewhat simpler to apply. However, the physical processes of urban heat island formation are fundamentally different under the influence of stable as compared to unstable atmospheres, so we might find more precision in models of ΔT if separate models are built for the different stability classes. This might be tested by comparing individual models for unstable, neutral, and stable Turner Classes to the combined classes model.
5. Account for differences in wind direction across the region, possibly by using wind data from networks such as Weather Underground or Weatherbug.

5 Conclusions

A single regression model was developed for predicting the temperature difference pattern across the Baltimore region for any summer weather conditions. Predictor variables were based on impervious cover, tree canopy cover, indices

of topography, and interactions of these cover and topography variables with atmospheric thermal stability, wind speed, antecedent rainfall, vapor pressure deficit, and weekend versus weekday. Tree cover generally led to cooler air temperatures, and impervious cover caused warmer air temperatures. The effect of land cover on temperature difference $\Delta \widehat{T}_{R\text{-}s}$ between a downtown reference location at R and temperatures at six other sites s differed greatly with different values of the Turner Class index of stability. Thus, interaction terms between stability and cover variables are included in our model.

The model explained about 50 % of the variance in temperature difference. Some of the unexplained variability is caused by a relatively few large residuals that are probably caused by short-term fluctuations in temperature at the measurement sites owing to times of rapid heating at some sites shortly after sunrise. Another part of the variance is caused by the short period of the averages of temperature and wind from the airport station. The portion of variance explained might be improved by the use of different averaging methods for the stability index, rather than giving equal weight to the most recent 3 hours as in the analysis here.

The regression model was applied to mapping temperature differences across the entire city of Baltimore and suburban areas. For most of the summer, temperatures differed by less than 5 °C over the area of nearly 1700 km^2. However, with clear skies and low wind speeds at night, urban minus rural temperatures, a measure of urban heat island intensity, differed by up to 12.4 °C. Topographic influences accounted for between 1.5 and 2.3 °C of the downtown to rural area difference.

For the 2 h of temperature patterns evaluated by Zhang et al. (2011) using a combined WRF and urban canopy model, our results were similar except that ours apparently did not account for bay breeze effects over part of our modeling domain, especially on one of the 2 days. The limitation of our relatively simple empirical method to deal with advection beyond 5 km did not seem to greatly affect results.

The methods used here might be applied in similar studies for other cities. However, in doing so, some care must be taken because of the strong inverse correlation between tree cover and impervious cover and the influence of topography on near-surface air temperature. The use of regression analysis requires cognizance of the physical processes at work and is not amenable to a "cookbook" approach. Models of this type could be useful in evaluating tree influences on temperature in a manner similar to that used by Ellis (2009). Direct application of the prediction equation developed here to other cities, using land cover, topography, and weather data (including wind speed and cloud cover from a primary station) from the other city to develop the input variables, has not yet been tested. There is considerable interest among urban foresters and urban planners for valuations of large-scale tree planting programs in reducing the warm season urban heat island effect, especially given the evidence of global warming that exacerbates the effects of high temperature on human health directly and by deterioration of air quality (Heisler and Brazel 2010; Nowak and Heisler 2010).

Acknowledgments Many individuals contributed in various ways to this study including Gregory Bacon, Kenneth Belt, Michelle Bunny, Richard Grant, Eric Greenfield, Sue Grimmond, Peter Groffman, Morgan Grove, John Hom, Karla Hyde, Andrew Lee, Jarlath O'Neil-Dunne, Richard Pouyat, Emma Powell, Hang Ryeol Na, Baohua Tao, Jeffrey Walton, and Yingjie Wang. John Stanovick, statistician with the USDA Forest Service, made numerous suggestions on the statistical analyses. This paper benefited from reviews of an earlier version by Anthony J. Brazel and Winston Chow. The Baltimore Ecosystem Study LTER, operating with contributions from the National Science Foundation grant DEB 0423476, provided some of the technical support staff and instrumentation. Two anonymous reviewers provided unusually helpful and detailed suggestions for improving the manuscript.

References

Allison PD (1999) Logistic regression using the SAS system: theory and application. SAS Institute, Cary

Ashie Y, Konob T (2011) Urban-scale CFD analysis in support of a climate-sensitive design for the Tokyo Bay area. Int J Climatol 31: 174–188

Baker LA et al. (2002) Urbanization and warming of Phoenix (Arizona, USA): Impacts, feedbacks and mitigation. Urban Ecosyst 6:183–203

Brazel AJ, Quatrocchi D (2005) Urban Climatology. In: Oliver J (ed) Encyclopedia of World Climatology. Springer, New York, pp 766-779

Brazel A, Selover N, Vose R, Heisler G (2000) The tale of two climates—Baltimore and Phoenix urban LTER sites. Clim Res 15:123–135

Brazel AJ, Fernando HJS, Hunt JCR, Selover N, Hedquist BC, Pardyjak E (2005) Evening transition observations in Phoenix, Arizona. J Appl Meteorol 44:99–112

Burnham KP, Anderson DR (2002) Model selection and multimodel inference: Second edition. Springer, New York

Chen F et al (2010) The integrated WRF/urban modeling system: development, evaluation, and applications to urban environmental problems. Int J Climatol 31:273–288

Cleugh H, Grimmond S (2012) Urban climates and global climate change. In: Henderson-Sellers A, McGuffie K (eds) The future of world's climate. Elsevier, Amsterdam, pp 47–76

Comrie A (2000) Mapping a wind-modified urban heat island in Tucson, Arizona (with comments on integrating research and undergraduate learning). BAMS, Bull Am Meteorol Soc 81:2417–2431

Ellis A (2009) Analyzing canopy cover effects on urban temperatures. M.S. Thesis, SUNY College of Environmental Science and Forestry, Syracuse, NY. Available from http://gradworks.umi.com/14/82/1482101.html

Fortuniak K, Klysik K, Wibig J (2006) Urban-rural contrasts of meteorological parameters in Lodz. Theor Appl Climatol 84:91–101. doi: 10.1007/s00704-005-0147-y

Georgescu M, Moustaoui M, Mahalov A, Dudhia J (2011) An alternative explanation of the semiarid urban area "oasis effect". J Geophys Res 116, D24113. doi:10.1029/22011JD016720

Gill GC (1983) Comparison Testing of Selected Naturally Ventilated Solar Radiation Shields: Report on Contract #NA-82-0A-A-266 with NOAA Data Buoy Office, Bay St. Louis, Miss. University of Michigan, Ann Arbor, Michigan

Grass D, Crane M (2008) The effects of weather and air pollution on cardiovascular and respiratory mortality in Santiago, Chile, during the winters of 1988–1996. Int J Climatol 28:1113–1126

Greenfield EJ, Nowak DJ, Walton JT (2009) Assessment of 2001 NLCD percent tree and impervious cover estimates. Photogramm Eng Remote Sens 75:1279–1286

Grimmond CSB (2011) Climate of cities. In: Douglas I, Goode D, Houck M, Wang R (eds) The Routledge handbook of urban ecology. Routledge, London, pp 103–119

Grimmond CSB, Oke TR (1999) Evapotranspiration rates in urban areas. In: Impacts of Urban Growth on Surface Groundwater Quality, International Union of Geodesy and Geophysics (IUGG) 99, Symposium HS5:235-243

Grimmond CSB et al (2010) Climate and more sustainable cities: climate information for improved planning and management of cities (producers/capabilities perspective). Procedia Environ Sci 1:247–274. doi:10.1016/j.proenv.2010.09.016

Harlan SH, Brazel AJ, Prashad L, Stefanov WL, Larsen L (2006) Neighborhood microclimates and vulnerability to heat stress. Soc Sci Med 63:2847–2863

Hartz DA, Brazel AJ, Heisler GM (2006) A case study in resort climatology of Phoenix, Arizona, USA. Int J Biometeorol 51:73–83

Heisler GM (1986) Energy savings with trees. J Arboric 12:113–125

Heisler GM, Brazel AJ (2010) The Urban Physical Environment: Temperature and Urban Heat Islands. In: Aitkenhead-Peterson J, Volder A (eds) Urban Ecosystem Ecology (Agronomy Monograph 55). American Society of Agronomy, Crop Science Society of America, Soil Science Society of America, Madison, WI, pp 29-56 [Available on-line http://www.treesearch.fs.fed.us/pubs/36427]

Heisler GM, et al (2000) A reference meteorological station for urban long-term ecological research, Baltimore Ecosystem Study. In: Third Urban Environment Symposium, Davis, CA, 14-18 Aug 2000 2000. American Meteorological Society, pp 189-190 [Available on-line http://www.beslter.org/pubs_browser.asp]

Heisler GM, Wang Y (2002) Applications of a human thermal comfort model. In: Fourth Symposium on the Urban Environment, Norfolk, VA, 20-24 May 2002. Am Meteorol Soc, Boston, MA, pp 70–71

Heisler G, et al (2007) Empirical modeling and mapping of below-canopy air temperatures in Baltimore, MD and vicinity. In: Seventh Urban Environment Symposium, San Diego, CA, Sep. 7 to 13, 2007. American Meteorological Society, Boston [Available online http://ams.confex.com/ams/pdfpapers/126981.pdf]

Heisler GM, Nowak D, Ellis A, Yesilonis I, Greenfield E (2010) Modeling influences of tree cover change on below-canopy urban air temperature, Ninth Symposium on the Urban Environment, August 2010, Keystone, CO. American Meteorological Society, Boston, MA. Abstract and recorded ppt presentation. http://ams.confex.com/ams/19Ag19BLT9Urban/techprogram/paper_172855.htm

Hirano Y, Yasuoka Y, Ichinose T (2004) Urban climate simulation by incorporating satellite-derived vegetation cover distribution into a mesoscale meteorological model. Theor Appl Climatol 79:175–184. doi:10.1007/s00704-004-0069-0

Kalkstein LS, Smoyer KE (1993) The impact of climate change on human health: some international implications. Experientia 49: 969–979

Krayenhoff ES, Voogt JA (2010) Impacts of urban albedo increase on local air temperature at daily-annual time scales: model results and synthesis of previous work. J Appl Meteorol Climatol 49: 1634–1648

Krayenhoff S, Stewart I, Oke TR (2009) Estimating thermal responsiveness of local-scale climate 'zones' with a numerical modeling approach. In: Joint Eighth Symposium on the Urban Environment and Timothy R. Oke Symposium, Phoenix, AZ. American Meteorological Society [Available on-line at http://ams.confex.com/ams/pdfpapers/149911.pdf]

Lindberg F, Grimmond CSB (2011) The influence of vegetation and building morphology on shadow patterns and mean radiant temperatures in urban areas: model development and evaluation. Theor Appl Climatol 105:311–323

Matzarakis A, Rutz F, Mayer H (2007) Modeling radiation fluxes in simple and complex environments–application of the Rayman model. Int J Biometeorol 51:323–334

Mills G (2007) Cities as agents of global change. Int J Climatol 27:1849–1857. doi:10.1002/joc.1604

Morris CJG, Simmonds I, Plummer N (2001) Quantification of the influences of wind and cloud on the nocturnal urban heat island in a large city. J Appl Meteorol 40:169–182

National Climatic Data Center (2011) U.S. Department of Commerce: National Environmental Satellite, Data, and Information Service http://www.ncdc.noaa.gov/oa/ncdc.html

NOAA (1998) Automated Surface Observing System (ASOS) User's Guide National Oceanic and Atmospheric Administration. http://www.nws.noaa.gov/asos/aum-toc.pdf

Nowak DJ, Heisler GM (2010) Air Quality Effects of Urban Trees and Parks National Recreation and Parks Association [http://www.nrpa.org/Content.aspx?id=4381]

Nowak DJ, Civeroloba KL, Rao ST, Sistla G, Luley CJ, Crane DE (2000) A modeling study of the impact of urban trees on ozone. Atmos Environ 34:1601–1613

Nowak DJ, Crane DE, Stevens JC (2006) Air pollution removal by urban trees and shrubs in the United States. Urban For Urban Green 4:115–123

Oke TR (1973) City size and the urban heat island. Atmos Environ 7: 769–779

Oke TR (1979) Review of Urban Climatology 1973-1976. World Meteorological Organization, Geneva

Oke TR (1982) The energetic basis of the urban heat island. Quart J R Meteorol Soc 108:1–24

Oke TR (1987) Boundary layer climates. Methuen, London and New York

Oke TR (1997) Urban climates and global environmental change. In: Thompson RD, Perry A (eds) Applied climatology: principles and practice. Routledge, London, pp 273–287

Oke TR (2006) Initial guidance to obtain representative meteorological observations at urban sites. World Meteorological Organization, Geneva

Oke TR (2011) Urban heat islands. In: Goode D, Houck M, Wang R (eds) Douglas I. The Routledge Handbook of Urban Ecology, London, pp 120–131

Oke TR, Johnson GT, Steyn DG, Watson ID (1991) Simulation of surface urban heat islands under 'ideal' conditions at night, Part 2: diagnosis of causation. Bound-Layer Meteorol 56:339–358

Panofsky HA, Dutton JA (1984) Atmospheric turbulence. John Wiley, New York

Rosenzweig C, Solecki WD, Slosberg RB (2006) Mitigating New York City's Heat Island with Urban Forestry, Living Roofs, and Light Surfaces. Columbia University Center for Climate Systems Research & NASA/Goddard Institute for Space Studies, New York

Roth M (2007) Review of urban climate research in (sub)tropical regions. Int J Climatol 27:1859–1973

Roth M, Emmanuel R, Ichinose T, Salmond J (2011) Editorial, ICUC-7 urban climate special issue. Int J Climatol 31:159–161

Runnalls KE, Oke TR (2000) Dynamics and controls of the near-surface heat island of Vancouver, British Columbia. Phys Geogr 21: 283–304

Sailor DJ (2011) A review of methods for estimating anthropogenic heat and moisture emissions in the urban environment. Int J Climatol 31: 189–199

SAS Institute Inc. (2003) SAS 9.1. SAS Institute Inc. http://www.sas.com/

Sikora TD, Young GS, Bettwy MJ (2010) Analysis of the Western shore Chesapeake Bay bay-breeze. Natl Weather Dig 34:55–64

Simpson JR (2002) Improved estimates of tree-shade effects on residential energy use. Energy Build 34:1067–1076

Stewart ID (2011) A systematic review and scientific critique of methodology in modern urban heat island literature. Int J Climatol 31:200–217

Stewart ID, Oke TR (2012) Local climate zones for urban temperature studies. BAMS, Bull Am Meteorol Soc. doi:10.1175/BAMS-D-11-00019.1

Stull RB (2000) Meteorology for scientists and engineers (Second Edition). Brooks/Cole, Pacific Grove

Taha H (1996) Modeling impacts of increased urban vegetation on ozone air quality in the South Coast air basin. Atmos Environ 30:3423–3430

Taha H, Douglas S, Haney J (1997) Mesoscale meteorological and air quality impacts of increased urban albedo and vegetation. Energy Build 25(2):169–177

Turner DB (1961) Relationships between 24-hour mean air quality measurements and meteorological factors in Nashville, Tennessee. J Air Pollut Control Assoc 11:483–489

Turner DB (1964) A diffusion model for an urban area. J Appl Meteorol 3:83–91

U.S. Department of the Interior (2011) National Land Cover Database 2006 (NLCD2006). U.S. Geological Survey. http://www.mrlc.gov/nlcd2006.php. Accessed December 30 2011

Voogt JA, Oke TR (2003) Thermal remote sensing of urban climates. Remote Sens Environ 86:370–384

Zhang D-L, Shou Y-X, Dickerson RR, Chen F (2011) Impact of upstream urbanization on the urban heat island effects along the Washington–Baltimore Corridor. J Appl Meteorol Climatol 50:2012–2029

Zhou W, Troy A (2008) An object-oriented approach for analysing and characterizing urban landscape at the parcel level. Int J Remote Sens 29:3119–3135